

## Pion production from the $pd \rightarrow d\pi^+n$ reaction at 585 MeV<sup>†</sup>

K. R. Hogstrom,\* G. S. Mutchler, T. R. Witten,<sup>†</sup> J. Hudomalj-Gabitzsch, J. M. Clement, R. D. Felder,  
W. H. Dragoset, W. P. Madigan, J. A. Buchanan, and G. C. Phillips  
T. W. Bonner Nuclear Laboratories, Rice University, Houston, Texas 77001

E. V. Hungerford, B. W. Mayes, L. Pinsky, L. Y. Lee, T. M. Williams, and J. C. Allred  
University of Houston, Houston, Texas 77004

(Received 6 May 1977)

Pion production from the reaction  ${}^2\text{H}(p, d\pi^+)n$  was measured in a kinematically complete experiment at an incident proton energy of 585 MeV. The deuteron was detected with a magnetic spectrometer fixed at 35°. The pion was detected at seven angles from 30° to 90° lab angle. The data exhibit a broad peak in the deuteron momentum spectrum that decreases in magnitude and shifts to greater momentum with increasing pion angle.

[NUCLEAR REACTIONS  ${}^2\text{H}(p, d\pi^+)n$ ,  $E = 585$  MeV; measured  $d^5\sigma/dp_1d\Omega_1d\Omega_2$ .]

### I. INTRODUCTION

The study of pion production from the deuteron, the most elementary nucleus, is of fundamental interest in understanding nucleon-nucleus pion production. Single pion production from deuterium can proceed via two-, three-, or four-body reactions:

$$p+d \rightarrow {}^3\text{H} + \pi^+, \quad (1a)$$

$$p+d \rightarrow {}^3\text{He} + \pi^0, \quad (1b)$$

$$p+d \rightarrow d + \pi^+ + n, \quad (1c)$$

$$p+d \rightarrow d + p + \pi^0, \quad (1d)$$

$$p+d \rightarrow p + \pi^+ + n + n, \quad (1e)$$

$$p+d \rightarrow p + p + n + \pi^0, \quad (1f)$$

$$p+d \rightarrow p + \pi^- + p + p. \quad (1g)$$

The two-body reactions (1a) and (1b) have been studied experimentally<sup>1-8</sup> and theoretically.<sup>9-15</sup> Ruderman<sup>9</sup> predicts that the  $\pi^+$  production for small momentum transfer to the neutron in reaction (1a) has its origin in the two nucleon  $pp \rightarrow d\pi^+$  reaction. Recent calculations by Fearing<sup>13</sup> which include distortion effects in the Ruderman model and the  $D$ -state part of the deuteron wave function<sup>13,14</sup> reproduce the shape and normalization of the data at 340, 470, and 590 MeV with the exception of the backward angles. Bhasin and Duck<sup>12</sup> have attempted to explain the backward angles using the Yao-Barry model<sup>15</sup> but were unable to account for the energy dependence of the backward rise of the cross section near 590 MeV.

Pion production involving three- and four-body reactions are largely unexplored except for the single arm data of Cochran *et al.*<sup>16</sup> and Hirt *et al.*<sup>17</sup> and one kinematically complete experiment on the reaction (1c) by Hungerford *et al.*<sup>18</sup> Because of the incident energy of the proton, one expects the qua-

sifree nucleon-nucleon interaction to dominate, so that

$$\sigma_d(\pi^+) \approx \sigma_p(\pi^+) + \sigma_n(\pi^+).$$

However, the data of Cochran *et al.* show that  $\sigma_d(\pi^+) < \sigma_p(\pi^+)$ , which they interpret as due to either a strong interference or a Glauber-type shadowing. The  $\sigma_d(\pi^+)/\sigma_d(\pi^-)$  ratio is found to be  $10.2 \pm 0.8$ , which agrees reasonably well with the isobar model prediction of 11.0. Such single arm data are not kinematically complete and hence may include many reaction mechanisms. In the kinematically complete experiment of Hungerford *et al.*, pion production from 800 MeV protons on deuterium was studied under conditions where the neutron in the deuteron target remains a spectator in the reaction. The pion production in such a reaction proceeds mainly through the mechanism proposed by Ruderman [Fig. 1(a)] and accounts for a large fraction of the total pion production in this kinematic region. The present experiment was limited to reactions (1c) and (1d) by requiring a deuteron to be present in the final state.

Because the deuteron is an isospin zero particle, a pion-nucleon final state in the (3, 3) resonance is isospin forbidden in reactions (1c) and (1d). This allows a study of  $\pi^+d$  interactions without a pion-nucleon resonance background.

Kinematical conditions were selected such that the neutron recoil momentum was 400 MeV/c or greater. In the one nucleon exchange (ONE) mechanism [Fig. 1(a)] this requires a 400 MeV/c or greater Fermi momentum for the nucleons in the deuteron, which is most probable if the nucleons are in a  $D$  rather than an  $S$  state. These conditions yield a small Fourier component of the deuteron wave function<sup>19</sup> which in turn reduces the contribution of the ONE amplitude which Hungerford *et al.* found to be dominant for small momentum transfer.

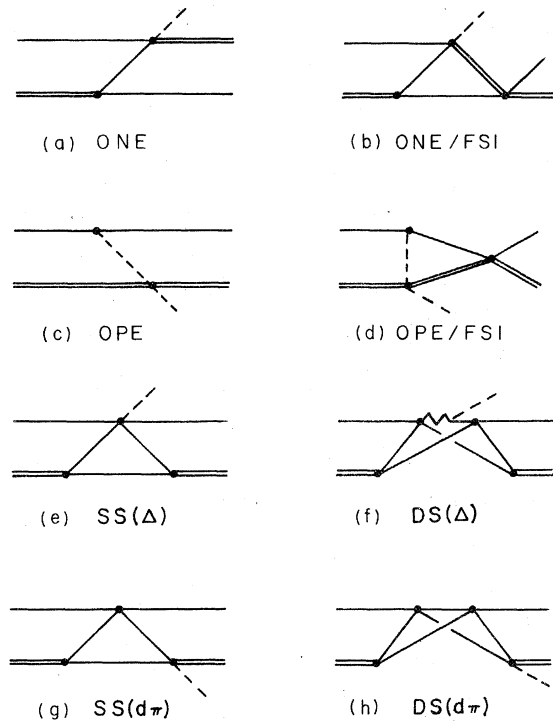


FIG. 1. Possible mechanisms for the  $pd \rightarrow d\pi n$  reaction at the present kinematical conditions. (a) One nucleon exchange, ONE; (b) one nucleon exchange with  $N$ - $N$  final state interaction, ONE/FSI; (c) one pion exchange, OPE; (d) one pion exchange with  $N$ - $N$  final state interaction, OPE-FSI; (e) impulse or single scattering SS ( $\Delta$ ); (f) double scattering with  $NN \rightarrow N\Delta$  DS ( $\Delta$ ); (g) single scattering with  $pp \rightarrow d\pi$  SS ( $d\pi$ ); (h) double scattering with  $pp \rightarrow d\pi$  DS ( $d\pi$ ).

Because such large Fermi components in the deuteron wave function are improbable, other mechanisms can be studied. Deuteron rescattering [Fig. 1(b)] via the  $nd$  interaction supplies the neutron with the required momentum transfer. Other favorable mechanisms are multiple scattering amplitudes with the reaction  $pp \rightarrow d\pi$  occurring at the last vertex [Fig. 1(g) single scattering (SS) ( $d\pi$ ) and Fig. 1(h) double scattering (DS) ( $d\pi$ )]. Other possible mechanisms are discussed in Ref. 22. The purpose of this experiment was to measure the cross sections from which the predominant reaction mechanisms can be inferred.

Since the SS ( $d\pi$ ) diagram was expected to be important, angle pairs were selected to measure dynamical effects in the region of 160 MeV ( $\pi^+d$ ) relative energy, where the  $pp \rightarrow \pi^+d$  cross section has a maximum. Data were taken at  $T_p = 585$  MeV with the deuteron detected at a fixed angle of  $35^\circ$  ( $\phi = 0$ ). The pion was detected at angles of 30, 35, 40, 50, 60, 70, and  $90^\circ$  ( $\phi = 180^\circ$ ). At the back-

ward angles, the  $\pi^+d$  relative energy does not reach 160 MeV. However, the relative energy does reach a maximum which still allows a study of the proposed mechanisms.

## II. DESCRIPTION OF THE EXPERIMENT

A schematic of the experimental apparatus is shown in Fig. 2. The external proton beam from the Space Radiation Effects Laboratory's 585 MeV synchrocyclotron was incident on a liquid deuterium target. The target cell was a 6.51 cm by 6.04 cm thin-walled Kapton cylinder. The entire system was enclosed in an evacuated target chamber and kept at a controlled temperature of  $24.9^\circ\text{K}$ , yielding an areal target density of  $0.966 \text{ g/cm}^2$ .

The beam was monitored by three separate systems. A multiwire proportional counter with an integrated output, located approximately 2 m downstream of the target, served as an on-line beam profile monitor<sup>20</sup> and insured that the beam position had not drifted. A calibrated 1.905 cm argon gas transmission ion chamber served as an absolute beam monitor, having a gain of  $214 \pm 11$  for 585 MeV protons for the ambient conditions of  $33^\circ\text{C}$ , 760 Torr. Because the cyclotron has a pulsed beam with a repetition rate of 55 Hz, the intensity during the beam bursts was too high for experimental purposes. A stretched beam with an average intensity of 30 pA was used with approximately 50% of the beam falling outside of the beam burst. All detectors were vetoed during the beam burst. The fraction of useful beam was then measured by a beam monitor scintillator telescope which counted both in an ungated and beam-burst-vetoed mode.

As a check of target thickness, beam intensity, and experimental techniques, the  $pd$  elastic cross section was measured and compared with the earlier results of Alder *et al.*<sup>21</sup> at  $35^\circ$  for the deuteron ( $71.2^\circ$  for the proton). The present cross section of  $23.3 \pm 2.0 \mu\text{b/sr}$  agrees within  $1\frac{1}{2}$  standard deviations with the previous value of  $25.9 \pm 0.5 \mu\text{b/sr}$ .

The scattered particles were detected by a spectrometer arm in coincidence with one of two time-of-flight (TOF) arms. The spectrometer, used solely for detecting the deuteron, remained at an angle of  $35^\circ$  throughout the course of the experiment. The spectrometer arm consisted of the beam-defining scintillators SS1 and SS2 which measured pulse height and time of flight, and served as fast strobes for the multiwire proportional counters (MWPC). The particle momentum was determined by measuring the incoming and outgoing rays using the four MWPC's in the spectrometer arm. The spectrometer subtended a solid angle of 5.5 msr at the central momentum of 800 MeV/c. The spectrometer momentum resolution was  $\delta p/p \approx 1.7\%$  [full

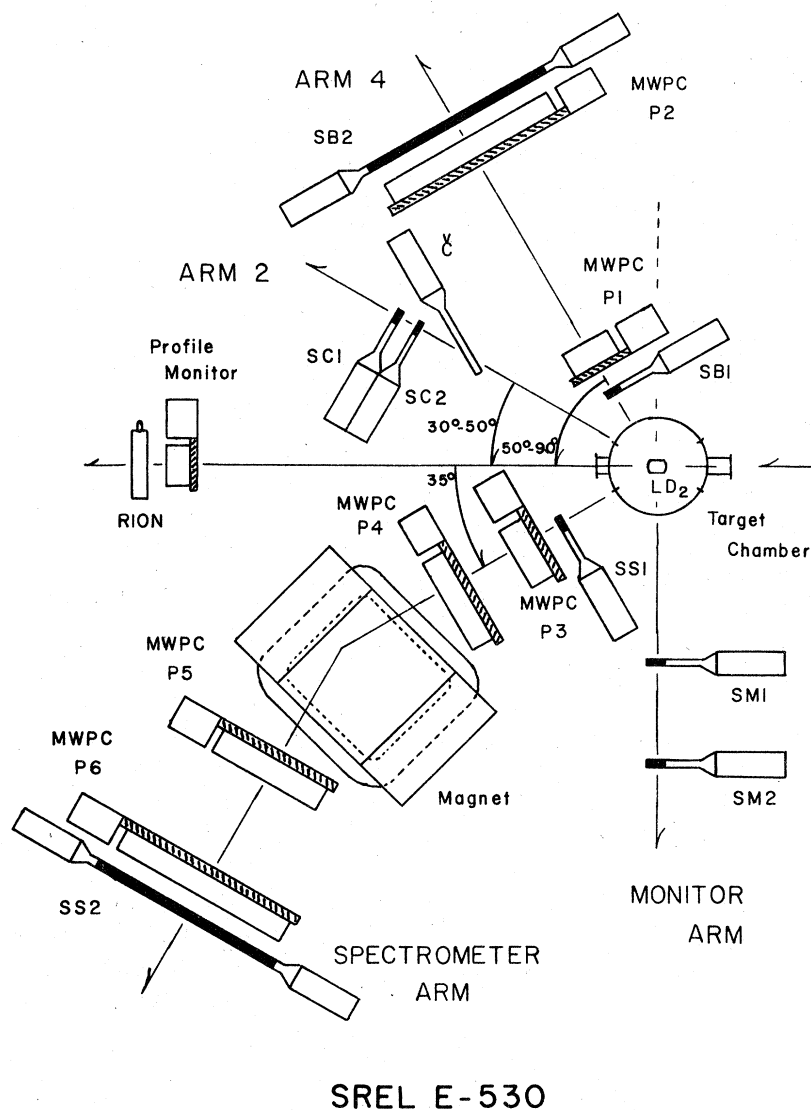


FIG. 2. Schematic of the experimental apparatus used for measuring the  $pd \rightarrow d\pi^+n$  cross section.

width at half maximum (FWHM)], as determined by using 1170 MeV/c elastically scattered deuterons.

The TOF arms, used solely for detecting pions or protons, are referred to as arm 2 and arm 4. One of these arms in coincidence with the spectrometer arm determined an event, subsequently referred to as tag 2 and tag 4 events, respectively. Arm 2 subtended a solid angle of 4.2 msr, while the arm 4 solid angle was 10.5 msr. Arm 2 spanned the pion angular range of  $30^\circ$  to  $50^\circ$  and arm 4, the angular range of  $50^\circ$  to  $90^\circ$ . Arm 4 contained two MWPC's which were used to measure the scattering angle of the pion (or proton). The angular resolution was approximately 2.5 mr.

Because arm 2 had a flight path of approximately 1.0 m compared to 2.7 m for arm 4, information

additional to the TOF was provided by a threshold Čerenkov detector. The Čerenkov radiator was 1.3 cm Plexiglas which has a  $\beta = 0.67$  threshold. This threshold separates the  $\beta$  of the pions from that of the protons for the kinematical conditions of the experiment.

The Rice MWPC detectors have been described in a previous work.<sup>22</sup> Each MWPC consists of an  $x, y$  grid of wires with a spacing of 2.5 mm. These detectors can sustain a count rate of 100 kHz/wire and have a multiple readout capability. The MWPC coordinates, along with the scintillator pulse heights, Čerenkov pulse height, time of flights, and tag identification were readout by an on-line PDP-11/45 computer and written onto magnetic tape. Tag 4 had priority over tag 2 in the

readout scheme.

This experiment measures five kinematical variables in the final state and thus completely determines the kinematics for three-body final states. These variables are determined by detecting two charged particles in coincidence where the momentum  $p_s$  and direction  $\theta_s$  are found for one charged particle passing through the spectrometer arm and the direction  $\theta_{\text{TOF}}$ ,  $\phi_{\text{TOF}}$  is found for the other charged particle passing through the time-of-flight (TOF) arm. By detecting the deuteron in the spectrometer arm, the observed final states are limited to reactions (1c), (1d), and to elastic scattering. Elastically scattered events are easily identified as they occur only at the elastic scattering angle pair and the deuteron momentum is greater than the maximum deuteron momentum for reactions (1c) and (1d). Data for reactions (1c) and (1d) are accumulated simultaneously and are separated by identification of either a charged pion or proton in the TOF arm. By measuring the time of flight in the TOF arm, three-body loci of deuteron momentum versus time of flight for the two reactions are obtained. Such loci are plotted in Fig. 3 where one can see that the time difference between the two loci is only a few nanoseconds. Signals from the Čerenkov detectors and pulse heights from the scintillators are used in addition to the time-of-flight measurement to separate reactions (1c) and (1d).

### III. DATA ANALYSIS

The  $d\pi^+n$  cross sections versus deuteron momentum were determined from the expression

$$\frac{d^5\sigma}{d\Omega_d d\Omega_{\pi^+} dp_d} = \frac{N_s / \epsilon_z \epsilon_{HB} \epsilon_{DT}}{N_0 n \Delta\Omega_s \Delta\Omega_{\text{TOF}} \Delta p_d^m |dp_d/dp_d^m|}, \quad (2)$$

where  $N_s$  is the number of  $d\pi^+n$  events in the momentum interval,  $p_d^m$  to  $p_d^m + \Delta p_d^m$ ;  $\epsilon_z$  is the detection efficiency for all MWPC's which nominally was about 90%;  $\epsilon_{HB}$  is the efficiency for all MWPC having distinguishable readouts which was typically 60%;  $\epsilon_{DT}$  is the live time of the electronics which nominally was about 99%;  $N_0$  is the number of protons incident on the liquid deuterium target;  $n$  is the target thickness of  $2.89 \times 10^{23}$  deuterons/cm<sup>2</sup>;  $\Delta\Omega_s \Delta\Omega_{\text{TOF}}$  is the solid angle in sr<sup>2</sup> of the experi-

$$\Delta\Omega_s \Delta\Omega_{\text{TOF}} = \frac{\iiint \Delta p_d \Delta\Omega_s' \Delta\Omega_{\text{TOF}}' K(\Omega_s, \Omega_{\text{TOF}}, p_d) T(\Omega_s, \Omega_{\text{TOF}}, p_d) d\Omega_s d\Omega_{\text{TOF}} dp_d}{\Delta p_d}, \quad (3)$$

where  $T$  is the transmission probability of a  $d\pi^+n$  final state for a deuteron of momentum  $p_d$  and direction  $\Omega_s$  and a pion of direction  $\Omega_{\text{TOF}}$  traversing all detectors in the experimental system after con-

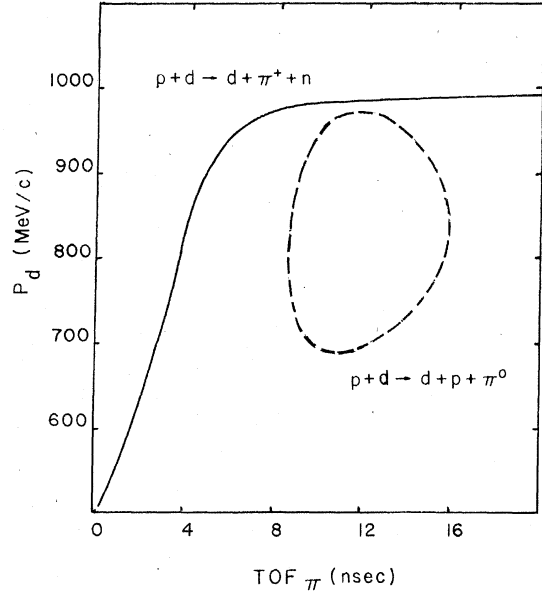


FIG. 3. Three-body loci for the  $d\pi^+n$  and  $d\pi^0$  final states, where the deuteron is detected by the spectrometer at  $35^\circ$  and the charged pion (proton) is detected by the TOF arm at  $50^\circ$ .

mental system as calculated by a Monte Carlo program;  $p_d^m$  is the momentum bin width of the data which is 20 MeV/c; and  $|dp_d/dp_d^m|$  corrects for energy loss of the deuterons in passing through the target cell, chamber windows, and the material in the spectrometer arm. Cross sections for each momentum interval are expressed at the median of that interval.

The bar over the fifth-order differential cross section indicates that the cross section is actually averaged over the experimental acceptance, namely that interval  $\Delta\Omega_s \Delta\Omega_{\text{TOF}} \Delta p_d$ , where  $\Delta p_d = \Delta p_d^m |dp_d/dp_d^m|$ . As the end of the kinematical locus is approached, kinematics prevents events for certain deuteron momentum from being emitted at all of the angles which would normally be accepted by the spectrometer arm. The cross section is averaged only over kinematically allowed and experimentally accepted regions. Therefore, the solid angle of the experimental system is given by

sidering multiple scattering, energy loss, and pion decay;  $K$  is a step function defining the kinematically allowed regions, being unity if  $\Omega_s$  and  $p_s$  for the deuteron and  $\Omega_{\text{TOF}}$  for the pion are kine-

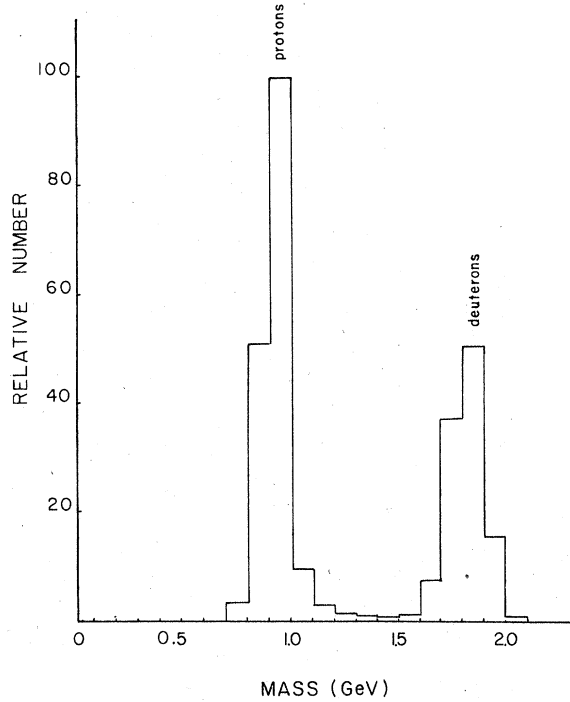


FIG. 4. Mass spectrum of particles through the spectrometer arm as calculated from Eq. (4).

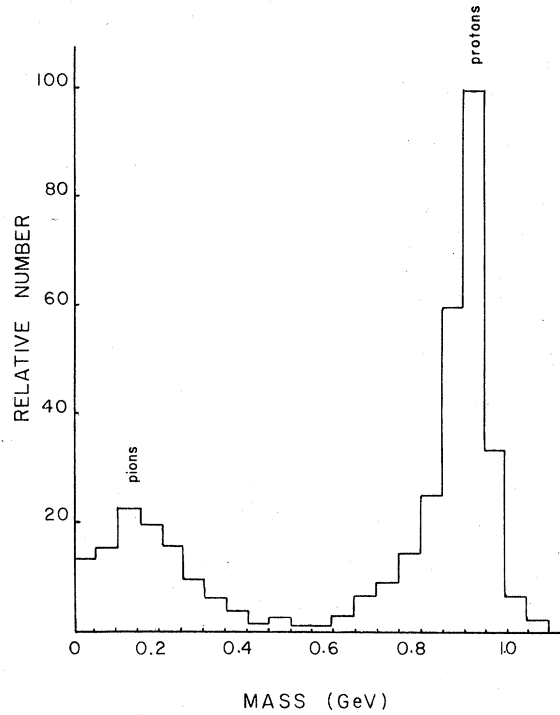


FIG. 5. Mass spectrum of particles through the TOF arm as calculated from Eq. (5).

matically allowed, zero otherwise; the  $\Delta\Omega'_s\Delta\Omega'_{\text{TOF}}$  are solid angle limits greater than those of the system such that any increase in the size of  $\Delta\Omega'_s$  or  $\Delta\Omega'_{\text{TOF}}$  will not change the value of the solid angle. The solid angle is evaluated by a Monte Carlo program which also averages  $\Delta\Omega_s\Delta\Omega_{\text{TOF}}$  over that part of the deuteron target intercepted by the proton beam.

Determination of the good events  $N_s$  was performed by individually analyzing those events in which all detectors had an acceptable readout. A series of cuts on the experimental quantities separated the  $d\pi^+n$  events from the competing reactions. Geometrical cuts were placed on the calculated point of origin for each event. Few events were eliminated here as the target was housed in an evacuated scattering chamber. Cuts were placed on the difference between the incoming and outgoing vertical slope and position of particles passing through the magnet so as to eliminate pole face scattering in the magnet. A two-dimensional cut was placed on the mass versus Čerenkov pulse height followed by a two-dimensional cut on the mass versus scintillator pulse height. These cuts

gave an estimated 99% pion-proton discrimination. The events passing all rejection criteria were associated with reactions (1c) and (1d) by identifying a deuteron in the spectrometer arm. The spectrometer momentum  $p_s$  was calculated assuming a uniform field model for the magnet. Then, knowing the velocity of the particle in the spectrometer,  $\beta_s$ , as determined from the scintillators, the particle mass was calculated by

$$m_s = \frac{p_s(1 - \beta_s^2)^{1/2}}{\beta_s}. \quad (4)$$

Proton-deuteron resolution was also obtained from pulse height in the 0.32 cm scintillator SS1. A two-dimensional cut of mass  $m_s$  versus pulse height identified the deuteron. Figure 4 shows a typical mass spectrum for the spectrometer.

Once a deuteron was detected in the spectrometer, it was assumed that only reactions (1c) or (1d) would produce a charged particle in the TOF arm. From conservation of energy and momentum, the mass of the particle scattered into the TOF arm can be calculated by

$$m_{\text{TOF}} = \frac{(E_T - E_d)^2 - (1076)^2 - T_b[T_b + 2(938.3)] - p_d^2 + 2p_d T_b [T_b + 2(938.3)]^{1/2} \cos \theta_d}{2[(E_T - E_d)\gamma_{\text{TOF}} - 1076 - \gamma_{\text{TOF}} \beta_{\text{TOF}} \{T_b [T_b + 2(938.3)]\}^{1/2} \cos \theta_{\text{TOF}} - p_d \cos \theta_{a,\text{TOF}}]}, \quad (5)$$

TABLE I.  $p+d \rightarrow d+\pi^++n$  cross sections in the laboratory frame.  $T_p=585$  MeV for  $\theta_d=35^\circ$  (tag 2 data).

$p_d$ (MeV/c)	$\frac{d^5\sigma}{d\Omega_{\pi^+}d\Omega_d dP_d}$ (nb/sr <sup>2</sup> MeV)	$p_d$ (MeV/c)	$\frac{d^5\sigma}{d\Omega_{\pi^+}d\Omega_d dP_d}$ (nb/sr <sup>2</sup> MeV)	$p_d$ (MeV/c)	$\frac{d^5\sigma}{d\Omega_{\pi^+}d\Omega_d dP_d}$ (nb/sr <sup>2</sup> MeV)
	$\theta_{\pi^+}=30^\circ$		$\theta_{\pi^+}=35^\circ$		$\theta_{\pi^+}=40^\circ$
627	147 ± 47	627	116 ± 26	626	78 ± 20
645	165 ± 33	645	102 ± 21	644	64 ± 16
663	180 ± 30	664	108 ± 19	663	119 ± 18
682	108 ± 22	682	110 ± 17	682	110 ± 16
700	142 ± 23	700	177 ± 20	700	83 ± 13
718	171 ± 24	719	161 ± 19	719	117 ± 15
736	176 ± 24	737	188 ± 20	737	120 ± 15
755	179 ± 23	756	184 ± 19	755	178 ± 17
773	225 ± 26	774	190 ± 19	774	181 ± 17
792	227 ± 25	792	220 ± 20	792	149 ± 15
811	211 ± 21	811	218 ± 20	811	167 ± 16
829	199 ± 23	830	212 ± 20	830	191 ± 17
848	118 ± 17	849	180 ± 18	848	168 ± 15
867	189 ± 22	868	185 ± 18	867	194 ± 16
886	139 ± 19	887	153 ± 16	886	191 ± 16
905	110 ± 17	906	131 ± 16	906	174 ± 16
925	65 ± 15	925	95 ± 14	925	124 ± 14
944	76 ± 17	945	93 ± 16	945	61 ± 11
964	65 ± 22	965	47 ± 15	965	48 ± 12
		985	46 ± 27		

where  $E_T$  is the total lab energy (3399 MeV),  $E_d$  is the deuteron lab energy,  $T_b$  is the kinetic energy of the incident proton,  $p_d$  is the deuteron lab momentum,  $\beta_{\text{TOF}}$  is the velocity of the unknown particle in the TOF arm,  $\gamma_{\text{TOF}} = (1 - \beta_{\text{TOF}}^2)^{-1/2}$ ,  $\theta_d$  is

the deuteron scattering lab angle,  $\theta_{\text{TOF}}$  is the scattering angle of the unknown particle in the TOF arm, and  $\theta_{d,\text{TOF}}$  is the angle between the deuteron and the unknown particle. Again the pulse height resolution between the pions and protons enabled

TABLE II.  $p+d \rightarrow d+\pi^++n$  cross section in the laboratory frame.  $T_p=585$  MeV for  $\theta_d=35^\circ$  (tag 4 data).

$p_d$ (MeV/c)	$\frac{d^5\sigma}{d\Omega_{\pi^+}d\Omega_d dP_d}$ (nb/sr <sup>2</sup> MeV)	$p_d$ (MeV/c)	$\frac{d^5\sigma}{d\Omega_{\pi^+}d\Omega_d dP_d}$ (nb/sr <sup>2</sup> MeV)	$p_d$ (MeV/c)	$p_d$ (MeV/c)	$p_d$ (MeV/c)	
	$\theta_{\pi^+}=50^\circ$		$\theta_{\pi^+}=60^\circ$				$\theta_{\pi^+}=70^\circ$
623	46 ± 16	644	28 ± 8	627	32 ± 13	682	31 ± 19
642	50 ± 12	663	34 ± 8	645	26 ± 8	700	17 ± 13
662	58 ± 11	681	42 ± 8	664	36 ± 10	719	23 ± 14
682	59 ± 11	700	39 ± 7	682	18 ± 5	737	48 ± 20
700	52 ± 9	718	45 ± 7	700	23 ± 6	755	26 ± 14
719	43 ± 8	737	58 ± 8	719	20 ± 5	774	25 ± 13
738	57 ± 9	755	50 ± 7	737	36 ± 7	792	24 ± 13
756	70 ± 10	774	48 ± 7	755	38 ± 7	811	53 ± 19
775	81 ± 10	792	64 ± 8	773	32 ± 7	829	46 ± 17
793	127 ± 12	811	63 ± 7	792	53 ± 8	848	50 ± 18
812	109 ± 11	829	85 ± 9	811	54 ± 8	867	69 ± 21
830	96 ± 10	848	85 ± 8	830	57 ± 8	886	67 ± 21
849	127 ± 12	867	102 ± 9	848	51 ± 7	905	76 ± 24
867	164 ± 13	886	133 ± 11	867	79 ± 9	924	87 ± 28
886	151 ± 13	905	131 ± 11	886 <sup>a</sup>	39 ± 26	944	93 ± 33
905	126 ± 12	925	146 ± 12	905 <sup>a</sup>	73 ± 24	964	79 ± 40
925	154 ± 14	944	145 ± 14	925 <sup>a</sup>	37 ± 42		
944	90 ± 12	963	98 ± 13	944 <sup>a</sup>	87 ± 42		
964	88 ± 14			964	84 ± 14		

<sup>a</sup> Background subtracted from data.

a two-dimensional mass versus pulse height cut to be made. Figure 5 shows results of the calculated mass spectrum in the TOF arm 4.

To insure internal consistency, the cross sections for tag 2 and tag 4 events were measured at the overlapping angle of  $50^\circ$  and found to agree within statistical errors.

#### IV. RESULTS AND DISCUSSION

Cross sections have been calculated in accordance with Eq. (2). The error bars are statistical arising from the number of  $d\pi^+n$  events and the determination of the wire plane efficiency  $\epsilon_{HB}$ . Statistical errors in the Monte Carlo calculation of solid angle are insignificant and have been neglected. Systematic errors in beam intensity and target thickness are estimated to be less than 10% as a result of the agreement of the  $pd$  elastic cross sections to previously measured values.

The cross sections versus deuteron momentum are listed in Tables I and II for the entire angular region spanned by the TOF arm detecting the pion. The deuteron is always detected at  $35^\circ$  and the pion angles range from  $30^\circ$  to  $90^\circ$ . No accidentals were

observed to contribute to the cross section; however, at  $70^\circ$  a correction was necessary at the higher momenta for protons misidentified as deuterons in the spectrometer. The  $70^\circ$  data were measured early in the experiment and this problem was corrected for the remaining angle pairs.

The three-body cross sections exhibit a definite peak in the deuteron momentum spectrum that decreases in magnitude and shifts to greater momentum with increasing pion angle. This angular dependence follows that of the maximum in the  $pp \rightarrow \pi^+d$  cross section which indicates that mechanisms containing a  $\pi^+d$  final state interaction [Figs. 1(g) and 1(h)] might contribute significantly; however, the angular dependence also follows the minimum in the final state neutron momentum which indicates that the ONE mechanism [Fig. 1(a)] also might contribute. Duck, Hogstrom, and Mutchler<sup>23</sup> have evaluated all of the diagrams shown in Fig. 1. They find that single and double scattering amplitudes with  $\pi$  production at one of the vertices [Figs. 1(f), 1(g), and 1(h)] provide a good global fit to the data. The calculated cross sections and data at  $\theta_\pi = 35^\circ, 50^\circ,$  and  $90^\circ$  are shown in Fig. 6.

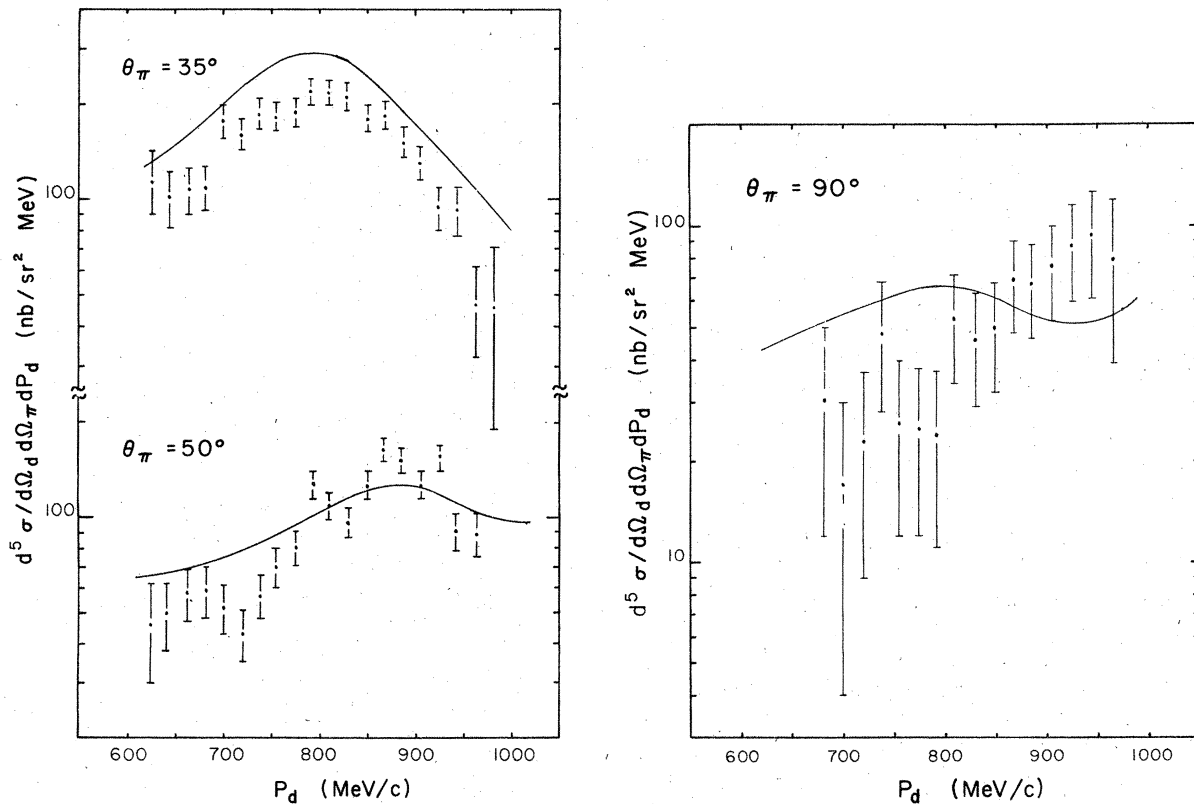


FIG. 6. Plots of the differential cross sections of Eq. (2) versus deuteron momentum. The deuteron is detected at  $35^\circ$  in all cases. The TOF arm and angle label each result accordingly. Error bars include only statistical errors. See Tables I and II for tabular results of the cross sections. The curves are from Ref. 23.

The calculations do not contain a normalization constant. Diagrams 1(a) and 1(b) may also contribute to the cross section but have not been included in Fig. 6. All other diagrams of Fig. 1 may be ignored.<sup>24</sup>

From their calculations Duck *et al.* find that the general magnitude of the differential cross section is given by diagram 1(f), the DS $\Delta$  process in which a  $\Delta$  resonance is produced in the first collision. The peak in the deuteron momentum spectrum is due to the SS ( $d\pi$ ) amplitude with the pion produced at the last vertex through the  $pp-d\pi$  reaction [Fig. 1(g)]. This must be combined coherently with the appropriate DS ( $d\pi$ ) amplitude [Fig. 1(h)]. A cancellation between SS ( $d\pi$ ) and DS ( $d\pi$ ) occurs and the magnitude of these two terms is sensitive to the range parameter of the nucleon-nucleon scattering amplitude. ( $R=0.425$  fm is used in the calculation; see reference 23 for details.) Finally, the DS ( $\Delta$ ) and DS ( $d\pi$ )-DS ( $d\pi$ ) cross sections are combined incoherently to give a reasonable fit to the data over the entire angular range.

All of the contributing diagrams are of second order, e.g., contain at least two vertices, so that in principle, off-shell amplitudes may be investigated. In addition, because of the large momentum transfers involved, one should also investigate

the effect of nuclear isobar components in the deuteron wave function. The calculations of Duck *et al.* are a preliminary attempt to extend Glauber theory to reactions and pion production.

Data exist at angles where the ONE mechanism is dominant. The data presented here are in the region of phase space where the ONE mechanism appears to be small. It would be interesting to connect these two regions by extending the angular distribution of the reaction to regions of intermediate momentum transfer where the SS and the ONE amplitudes become large enough to dominate the DS ( $\Delta$ ) amplitude.

#### ACKNOWLEDGMENTS

We thank Joe Lo, Ken Koester, and James Thomasson for their help in conducting the experiment. We would like to express our gratitude to Dr. R. Siegel and the entire staff of the Space Radiation Effects Laboratory for their support and cooperation. The Space Radiation Effects Laboratory is supported by the National Aeronautics and Space Administration, the Commonwealth of Virginia, and the National Science Foundation, whose support is gratefully acknowledged.

- 
- \*Present address: University of New Mexico School of Medicine, Albuquerque, New Mexico.  
 †Work supported in part by U. S. Energy Research and Development Administration.  
 ‡Present address: Kent State University, Kent, Ohio.  
<sup>1</sup>W. J. Frank, K. C. Randel, R. Madey, and B. J. Moyer, Phys. Rev. **94**, 1716 (1954).  
<sup>2</sup>K. C. Bandtel, W. J. Frank, and B. J. Moyer, Phys. Rev. **106**, 802 (1957).  
<sup>3</sup>D. Harting *et al.*, Phys. Rev. **119**, 1716 (1960).  
<sup>4</sup>A. V. Crewe *et al.*, Phys. Rev. **118**, 1091 (1960).  
<sup>5</sup>N. E. Booth, Phys. Rev. **132**, 2305 (1963).  
<sup>6</sup>K. R. Chapman *et al.*, Nucl. Phys. **57**, 499 (1964).  
<sup>7</sup>K. Gabathuler *et al.*, Nucl. Phys. **B40**, 32 (1972).  
<sup>8</sup>W. Dolhkopf *et al.*, Nucl. Phys. **A217**, 381 (1973).  
<sup>9</sup>M. Ruderman, Phys. Rev. **87**, 383 (1952).  
<sup>10</sup>C. H. Q. Ingram, N. W. Tanner, J. J. Domingo, and J. Rohlin, Nucl. Phys. **B31**, 331 (1971).  
<sup>11</sup>G. W. Barry, Phys. Rev. D **7**, 1441 (1973).  
<sup>12</sup>V. S. Bhasin and I. M. Duck, Phys. Lett. **46B**, 309 (1973).  
<sup>13</sup>H. W. Fearing, Phys. Rev. C **11**, 1210 (1975).  
<sup>14</sup>H. W. Fearing, Phys. Rev. C **11**, 1493 (1975).  
<sup>15</sup>T. Yao, Phys. Rev. **134**, 3454 (1964); G. Barry, Ann. Phys. (N.Y.) **73**, 482 (1972).  
<sup>16</sup>D. R. F. Cochran *et al.*, Phys. Rev. D **6**, 3085 (1972).  
<sup>17</sup>W. Hirt, E. Heer, M. Martion, E. G. Michaelis, C. Serre, P. Skarek, and B. T. Wright, CERN Report No. 69-24, 1964 (unpublished).  
<sup>18</sup>E. V. Hungerford *et al.*, in *Proceedings of the Topical Conference on Meson-Nuclear Physics, Pittsburgh 1976*, edited by P. D. Barnes, R. A. Eisenstein, and L. S. Kisslinger (AIP, New York, 1976), AIP No. 33, p. 448.  
<sup>19</sup>M. J. Moravcsik, Nucl. Phys. **7**, 113 (1958); Y. Yamaguchi and Y. Yamaguchi, Phys. Rev. **95**, 1635 (1954).  
<sup>20</sup>J. A. Buchanan, W. Madigan, and G. C. Phillips (unpublished).  
<sup>21</sup>J. C. Alder *et al.*, Phys. Rev. C **6**, 2010 (1972).  
<sup>22</sup>J. A. Buchanan *et al.*, Nucl. Instrum. Methods **99**, 159 (1972).  
<sup>23</sup>I. Duck, K. R. Hogstrom, and G. S. Mutchler (unpublished).  
<sup>24</sup>Diagrams 1(c) and 1(e) are the same but with different interaction bubbles.